

# Spontaneous rotational symmetry breaking in $\text{KTaO}_3$ interface superconductors

Guanqun Zhang,<sup>1,\*</sup> Lijie Wang,<sup>1,\*</sup> Jinghui Wang,<sup>2,\*</sup> Guangyi Huang,<sup>1</sup> Huanyi Xue,<sup>1</sup> Yueshen Wu,<sup>2</sup> Yanru Song,<sup>3,†</sup> Zhenghua An,<sup>1,4</sup> Changlin Zheng,<sup>1</sup> Jun Li,<sup>2,‡</sup> Yan Chen,<sup>1</sup> and Wei Li<sup>1,§</sup>

<sup>1</sup>*State Key Laboratory of Surface Physics and Department of Physics, Fudan University, Shanghai 200433, China*

<sup>2</sup>*School of Physical Science and Technology, ShanghaiTech University, Shanghai 201210, China*

<sup>3</sup>*Center for Transformative Science, ShanghaiTech University, Shanghai 201210, China*

<sup>4</sup>*Institute for Nanoelectronic Devices and Quantum Computing, Fudan University, Shanghai 200433, China*

(Dated: November 23, 2021)

We report the observation of spontaneous rotational symmetry breaking of the superconductivity at the interface of  $\text{YAlO}_3/\text{KTaO}_3$  with a superconducting transition temperature of 1.86 K. Both the magnetoresistance and upper critical field in an in-plane field manifest striking asymmetric twofold oscillations deep inside the superconducting state, whereas the anisotropy vanishes in the normal state, demonstrating that this is an intrinsic property of the superconducting phase. We attribute this behavior to the mixed-parity superconducting state, which is an admixture of *s*-wave and *p*-wave pairing components induced by strong spin-orbit coupling. Our work demonstrates the unconventional nature of the pairing interaction in the  $\text{KTaO}_3$  interface superconductor, and provides a new platform to clarify a delicate interplay of electron correlation and spin-orbit coupling.

The intriguing properties of interface superconductivity has been a central theme in condensed matter physics in recent years [1]. Indeed, the presence of inversion symmetry breaking and the interfacial coupling between two constitute materials are expected to promote the strong interplay between electron correlations, providing an ideal platform for unveiling the inherent pairing mechanism of unconventional superconductivity and promising avenues for the development of superconductor-based devices [2–4]. The prototype interface superconductivity has been experimentally observed at the interface of  $\text{LaAlO}_3/\text{SrTiO}_3$  with a superconducting transition temperature ( $T_c$ ) of 250 mK [5]. Subsequently, the superconductivity at the interface of  $\text{La}_{1.55}\text{Sr}_{0.45}\text{CuO}_4/\text{La}_2\text{CuO}_4$  has been also observed [6]. Interestingly, monolayer FeSe films grown on  $\text{SrTiO}_3$  substrates show superconductivity above 100 K by compared to their bulk with a  $T_c$  below 8 K [7–9]. This suggests that the electron correlations and the coupling at the interface cooperatively contribute to the remarkable enhancement of superconductivity [10].

Very recently, unexpected crystalline-orientation dependent superconductivity has been experimentally observed at the interface between  $\text{EuO}$  (or  $\text{LaAlO}_3$ ) and  $\text{KTaO}_3$  ( $T_c \sim 2$  K) [11–13], which shows near two orders of magnitude enhancement in  $T_c$  compared to its three-dimensional counterpart [14]. This findings suggest that superconductivity at  $\text{KTaO}_3$  interfaces is an intrinsic interface property. In particular, we conjecture that the dimensional reduction induces strong electron correlations, which play a crucial role in the spontaneous symmetry breaking of the ground state of (111)-oriented  $\text{KTaO}_3$  interfaces. Interestingly, an indication of broken symmetry phase with a strong in-plane anisotropy of the electrical resistance has been reported at the interface of ferromagnetic  $\text{EuO}$  and  $\text{KTaO}_3$  [11]. Theoretically, this symmetry breaking phase in  $\text{EuO}/\text{KTaO}_3$  may come from the joint

effect of the ferromagnetic order in  $\text{EuO}$  and the strong electron correlation at the interface [15], leading the intrinsic nature of rotational symmetry breaking in  $\text{KTaO}_3$  interface superconductors to be elusive.

In this Letter, we carry out an experimental study on nonmagnetic  $\text{YAlO}_3$  thin films with a wide-band gap of 7.9 eV grown on the polar  $\text{KTaO}_3(111)$  substrates. This gap is significantly larger than that of  $\text{LaAlO}_3$  (5.6 eV) [16], enabling strong confinement potential to restrict the interfacial conducting electrons to a thinner interfacial layer, thus prompting an intriguing quantum behaviors at their interface [17]. Electrical transport measurements on the as-grown films reveal two-dimensional superconductivity with a  $T_c$  of 1.86 K, and a superconducting layer thickness of 4.5 nm. By tuning the in-plane azimuthal angle  $\varphi$ -dependent magnetic field, both the magnetoresistance and upper critical field display pronounced asymmetric twofold oscillations deep inside the superconducting state, while they vanish in the normal state. These results unambiguously demonstrate that the anisotropy with in-plane rotational symmetry breaking is an intrinsic property of the superconducting phase in  $\text{YAlO}_3/\text{KTaO}_3$ . We thus classify the inversion symmetry breaking  $\text{KTaO}_3$  interface superconductor as a mixed-parity unconventional superconductivity with an admixture of *s*-wave and *p*-wave pairing components.

The  $\text{YAlO}_3/\text{KTaO}_3$  heterostructures are prepared by depositing  $\text{YAlO}_3$  films on a (111)-oriented  $\text{KTaO}_3$  single crystal substrate using pulsed laser deposition (see Supplementary Materials [18]). Atomic force microscopy characterizations show that the surface of  $\text{KTaO}_3$  substrates and  $\text{YAlO}_3$  films are atomically flat (see Fig. S1 [18]). X-ray diffraction confirms the absence of epitaxial peaks of  $\text{YAlO}_3$  (see Fig. S2 [18]), thus suggesting that the  $\text{YAlO}_3$  film is not in a well-defined crystalline phase. The microstructure of the interface is further examined by aberration-corrected scanning transmission electron

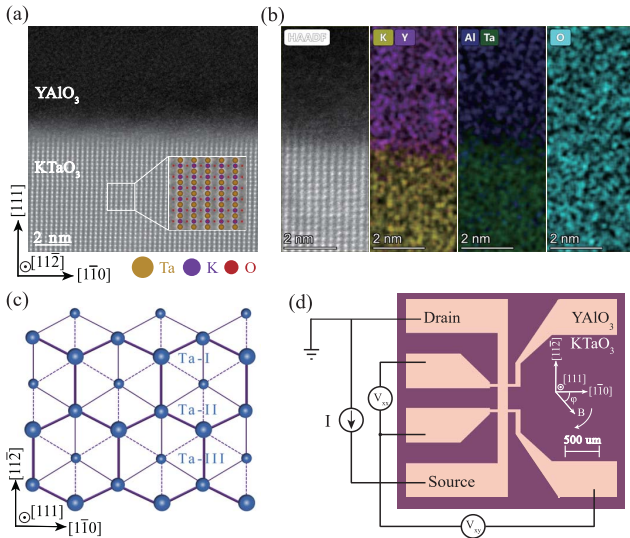


FIG. 1. (a) HAADF-STEM image of YAlO<sub>3</sub>/KTaO<sub>3</sub> viewed along the [112] zone axis. The inset shows the enlarged HR-STEM image of KTaO<sub>3</sub> overlapped with atomic configuration (colored). (b) HR-STEM image and the corresponding EDS elemental mapping of interface. (c) Distribution of Ta<sup>5+</sup> ions along the [111] crystal axis of KTaO<sub>3</sub>(111) surface. Ta<sup>5+</sup> ions are shown with progressively smaller sizes in the three adjacent (111) planes, which are labeled as Ta-I, Ta-II, and Ta-III, respectively. (d) Hall bar structure on YAlO<sub>3</sub>/KTaO<sub>3</sub>(111) heterostructure. Here,  $\varphi$  is defined as the in-plane azimuthal angle between the applied magnetic field  $B$  and the [1̄10]-axis of the lattice, shown in the inset of (d).

microscopy (STEM). From the high angle annular dark field (HAADF)-STEM image [see Fig. 1(a)], it can be seen that the amorphous phase YAlO<sub>3</sub> thin film is grown on the KTaO<sub>3</sub>(111) substrate. Looking at the sample from a larger field of view, the thickness of the YAlO<sub>3</sub> film is found to be about 60 nm. High-resolution (HR)-STEM imaging [Fig. 1(a)] and energy dispersive X-ray spectroscopy (EDS) elemental mapping [Fig. 1(b)] demonstrate that the interface of YAlO<sub>3</sub>/KTaO<sub>3</sub> is clearly resolved structurally and chemically, confirming the high-quality growth of the YAlO<sub>3</sub> films on the KTaO<sub>3</sub> substrates.

Fig. 2(a) shows the temperature-dependent sheet resistance  $R_s$  on two representative as-grown YAlO<sub>3</sub> thin films (Samples #1 and #2 with growth temperatures of 780 °C and 650 °C, respectively) with the Hall bar structure, schematically illustrated in Fig. 1(d). A typical metallic behavior is visible in a wide temperature range, indicating that a two-dimensional electron gas is formed at their interface induced by the combination of the polar KTaO<sub>3</sub> and oxygen vacancies. The transverse Hall resistance  $R_{xy}$  is obtained from Hall measurements at 5 K, and reveals that the charge carriers in the YAlO<sub>3</sub>/KTaO<sub>3</sub> are electrons. The estimated carrier density is about  $1.45 \times 10^{14} \text{ cm}^{-2}$  and  $6.62 \times 10^{13} \text{ cm}^{-2}$  for Samples #1 and #2, respectively. The electron mo-

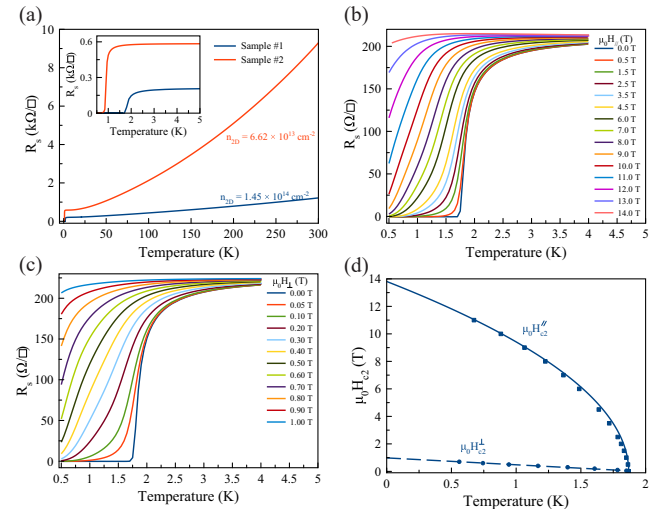


FIG. 2. (a) Electrical resistance ( $R_s$ ) as a function of temperature at zero magnetic field for two representative YAlO<sub>3</sub>/KTaO<sub>3</sub> heterostructures (Samples #1 and #2). Low temperature dependence of  $R_s$  is illustrated in the inset of (a). Magnetoresistance for fields (b) parallel and (c) perpendicular to the plane surface of Sample #1. (d) Temperature dependence of the upper critical field  $\mu_0 H_{c2}$ .

bility for Samples #1 and #2 is thus  $193.6 \text{ cm}^2 \text{V}^{-1} \text{s}^{-1}$  and  $159.7 \text{ cm}^2 \text{V}^{-1} \text{s}^{-1}$ . These results are highly reproducible and reasonably consistent with previous electrical transport studies on EuO/KTaO<sub>3</sub> [11, 12] and LaAlO<sub>3</sub>/KTaO<sub>3</sub> [11, 13]. Remarkably, as the temperature is further decreased, the resistance  $R_s$  undergoes a narrow and sharp transition with a transition width of less than 0.5 K to a zero-resistance state, signaling the appearance of superconductivity at the interface of YAlO<sub>3</sub>/KTaO<sub>3</sub>. The critical temperature is  $T_c = 1.86 \text{ K}$  and  $0.92 \text{ K}$  for Samples #1 and #2, respectively, as defined by where the resistance is at the midpoint of the normal electrical resistance at 5 K, i.e.  $R_s(T_c) = 0.5 \times R_s(5 \text{ K})$ .

To further characterize the superconducting behaviors in YAlO<sub>3</sub>/KTaO<sub>3</sub>, we measure the magnetoresistance  $R_s(\mu_0 H)$  (here,  $\mu_0$  is the vacuum permeability) at various temperatures between 0.5 K and 5 K with fields parallel ( $\mu_0 H_{\parallel}$ ) and perpendicular ( $\mu_0 H_{\perp}$ ) to the plane surface of Sample #1, as shown in Figs. 2(b) and 2(c), respectively. The fundamental superconducting behavior is clearly resolved. Indeed, the magnetoresistance  $R_s(\mu_0 H)$  varies differently with  $\mu_0 H_{\parallel}$  and  $\mu_0 H_{\perp}$ , and both the superconducting critical fields  $\mu_0 H_{c2}^{\parallel}$  and  $\mu_0 H_{c2}^{\perp}$  parallelly shift to a lower value with the increase of the field, where  $\mu_0 H_{c2}$  are evaluated at the midpoints of the normal-state resistance at 5 K. These results provide an indication of a two-dimensional superconducting feature in YAlO<sub>3</sub>/KTaO<sub>3</sub>. The temperature-dependent upper critical fields  $\mu_0 H_{c2}$  are shown in Fig. 2(d) and are well fitted by the phenomenological two-dimensional Ginzburg-

Landau (G-L) model [19]:  $\mu_0 H_{c2}^\perp(T) = \frac{\Phi_0}{2\pi\xi_{GL}^2}(1 - \frac{T}{T_c})$  and  $\mu_0 H_{c2}^\parallel(T) = \frac{\Phi_0\sqrt{12}}{2\pi\xi_{GL}d_{SC}}\sqrt{1 - \frac{T}{T_c}}$ , where  $\Phi_0$ ,  $\xi_{GL}$ , and  $d_{SC}$  denote a flux quantum, the in-plane superconducting coherence length at  $T = 0$  K, and the effective thickness of superconductivity, respectively. Using the extrapolated  $\mu_0 H_{c2}^\perp(0) = 0.98$  T and  $\mu_0 H_{c2}^\parallel(0) = 13.81$  T, we find  $\xi_{GL} = 18.4$  nm and  $d_{SC} = 4.5$  nm, where  $\xi_{GL}$  is significantly larger than  $d_{SC}$ , suggesting a two-dimensional nature of superconductivity. Additionally, the in-plane  $\mu_0 H_{c2}^\parallel(0)$  is substantially larger than the Pauli-paramagnetic pair-breaking field  $B_P \approx 3.46$  T based on the BCS theory in the weak-coupling limit [20, 21]. High values of  $\mu_0 H_{c2}^\parallel(0)$  exceeding  $B_P$  can be realized in the presence of strong spin-orbit coupling owing to the elastic scattering, which results in the suppression of spin paramagnetism effects. The violation of this paramagnetic limit is a common phenomenon in interface superconductors [11, 13, 22–25], especially when the superconducting layer thickness is in the range  $d_{SC} < 20$  nm. However, the mechanism for realizing  $\mu_0 H_{c2}^\parallel(0)$  value in excess of  $B_P$  remains an open question [11]. Furthermore, the thickness of the superconducting layer in  $\text{YAlO}_3/\text{KTaO}_3(111)$  is  $d_{SC} = 4.5$  nm, which is the thinnest value recorded in the heterointerface superconductors so far [11, 13, 22–26]. This result is intuitively expected, since the strong confinement potential induced by  $\text{YAlO}_3$  significantly restricts the superconducting electrons to a thinner superconducting layer [17]. On the other hand, the out-of-plane polar angle  $\theta$ -dependent critical field  $H_{c2}^\theta$  at 1.5 K quantitatively verifies the behavior expected from a two-dimensional structure in  $\text{YAlO}_3/\text{KTaO}_3$ , as shown in Fig. S3 [18]. The  $\theta$ -dependent  $\mu_0 H_{c2}^\theta$  are well fitted by the two-dimensional Tinkham formula and the three-dimensional anisotropic G-L model, given by  $\frac{H_{c2}^\theta |\cos \theta|}{H_{c2}^\perp} + \left(\frac{H_{c2}^\theta \sin \theta}{H_{c2}^\parallel}\right)^2 = 1$  and  $\left(\frac{H_{c2}^\theta \cos \theta}{H_{c2}^\perp}\right)^2 + \left(\frac{H_{c2}^\theta \sin \theta}{H_{c2}^\parallel}\right)^2 = 1$ , respectively [27, 28]. A cusp-like peak is clearly observed at  $\theta = 90^\circ$  (see Fig. S3 [18]), which is well described by the two-dimensional Tinkham model, as frequently observed in interface superconductivity [5, 11, 29] and layered transition metal dichalcogenides [28, 30].

Since the superconductivity in  $\text{YAlO}_3/\text{KTaO}_3$  is two-dimensional, the Berezinskii-Kosterlitz-Thouless (BKT) transition describes superconducting phase coherence [31, 32]. Here, the BKT transition temperature defines the vortex unbinding transition, and can be determined using current-voltage ( $I$ - $V$ ) measurements as a function of temperature  $T$ , as shown in Fig. 3(a). Below  $T_c$ , we find a critical current  $I_c$ , whose value decreases with increase in temperature. The maximal value of  $I_c$  is 330 A at 0.5 K, which is substantially larger than that observed in  $\text{EuO}/\text{KTaO}_3$  [11] and  $\text{LaAlO}_3/\text{KTaO}_3$  [13]. Such a high critical current value originates from the high charge carrier concentration

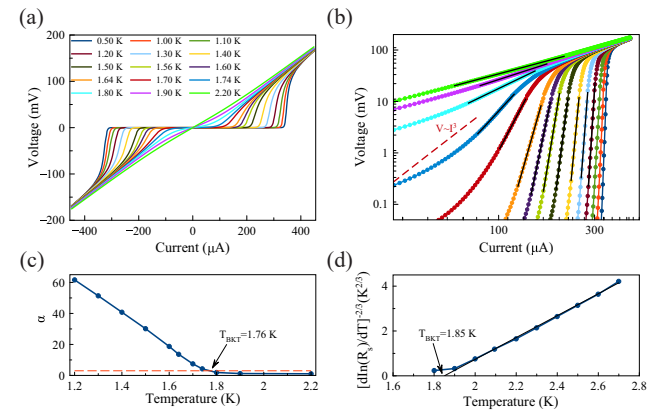


FIG. 3. (a) Temperature-dependent  $I$ - $V$  measurements. (b) Corresponding logarithmic scale representation of (a). The long red dashed line denotes the  $V \sim I^3$  dependence. (c) Temperature dependence of the power-law exponent  $\alpha$ , as deduced from the fits shown in (b). (d)  $R_s(T)$  dependence of the same sample, plotted on a  $[d \ln(R_s)/dT]^{-2/3}$  scale.

(about  $1.45 \times 10^{14}$  cm $^{-2}$ ) confined in a thinner superconducting layer of  $\text{YAlO}_3/\text{KTaO}_3$ , promising for large-scale applications in superconductor-based devices. In Fig. 3(b), we also plot the characteristics  $I$ - $V$  on a log-log scale, and observe that the slope of the  $I$ - $V$  curve smoothly evolves from the normal ohmic state,  $V \propto I$ , to a steeper power law resulting from the current exciting free-moving vortices,  $V \propto I^{\alpha(T)}$ , with  $\alpha(T_{BKT}) = 3$ . In Fig. 3(c), a value  $T_{BKT} = 1.76$  K is interpolated, which is consistent with  $T_c$  as defined in Fig. 2(a). In addition, close to  $T_{BKT}$ , an  $R_s = R_0 \exp[-b(T/T_{BKT} - 1)^{-1/2}]$  dependence, where  $R_0$  and  $b$  are material parameters, is expected [33]. As shown in Fig. 3(d), the measured  $R_s(T)$  is also consistent with this behavior and yields  $T_{BKT} = 1.85$  K, in good agreement with the analysis of the  $\alpha$  exponent.

Next, we discuss the in-plane anisotropy of superconductivity in  $\text{YAlO}_3/\text{KTaO}_3$  using an in-plane azimuthal angle  $\varphi$ -dependent magnetoresistance, where  $\varphi$  is defined as the azimuthal angle between the magnetic field and the  $[1\bar{1}0]$ -axis of the lattice, as indicated in Fig. 1(d). In the normal state [ $T = 5$  K in Fig. 4(a)], the magnetoresistance  $R_s$  is found to be essentially independent of  $\varphi$ , displaying isotropic behavior. While in the superconducting state [ $T = 1.5$  K in Fig. 4(a)], we observe a pronounced asymmetric twofold oscillations of the magnetoresistance  $R_s$  [see Fig. 4(b)]. In this case, the anisotropic magnetoresistance  $R_s$  attains the maximum value when the magnetic field is directed along the  $[11\bar{2}]$ -axis ( $\varphi = 90^\circ$ ) and becomes minimum when the field is directed along the  $[1\bar{1}0]$ -axis ( $\varphi = 0^\circ$ ) (also see Fig. S4 [18]). Considering that the existence of striking asymmetric twofold oscillations in magnetoresistance manifests deep inside the superconducting region and vanishes in the normal state, we can straightforwardly rule out the possibilities of ex-

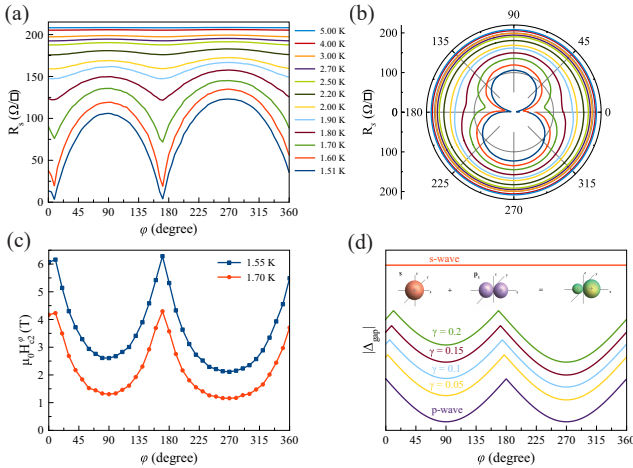


FIG. 4. (a) In-plane angular-dependent magnetoresistance  $R_s$  at various temperatures for an applied field of 3 T. (b) Polar plots of the data in (a). (c) In-plane angular-dependent  $\mu_0H_{c2}$  at various temperatures. (d) Theoretical evaluations of mixed-parity superconducting gap  $|\Delta_{gap}|$  with an admixture of  $s$ -wave  $\Delta_s$  and  $p$ -wave  $\Delta_p$  components. The  $\Delta_s/\Delta_p$  ratio is denoted as  $\gamma$ . A schematic diagram illustrating the admixture of  $s+p$ -wave pairing orbital symmetry is given in the inset of (d).

trinsic contributions, such as the magnetic field induced Lorentz force effect [34] and the electronic band structure inherent to the  $\text{KTaO}_3$  with respect to the underlying threefold lattice symmetry [35] [also see Fig. 1(c)], and thus demonstrate that this anisotropy is an intrinsic property of the superconducting phase in  $\text{YAlO}_3/\text{KTaO}_3$ .

To further reveal the twofold asymmetric superconductivity in  $\text{YAlO}_3/\text{KTaO}_3$  in terms of the superconducting gap structure, we extract the upper critical field  $\mu_0H_{c2}$  from the  $\varphi$ -dependent magnetoresistance  $R_s$  in the superconducting region. Interestingly, the in-plane  $\varphi$ -dependent  $\mu_0H_{c2}^\varphi$  also displays asymmetric twofold oscillations, providing additional strong evidence for the twofold rotational asymmetry of the superconductivity in  $\text{YAlO}_3/\text{KTaO}_3$ . In addition, the oscillation of  $\mu_0H_{c2}^\varphi$  has a  $\pi$  phase shift compared with that of the magnetoresistance  $R_s$  [see Fig. 4(a)] such that for the  $\varphi$  value where superconductivity is hardest to suppress,  $\mu_0H_{c2}^\varphi$  is the largest and the magnetoresistance  $R_s$  is the lowest [Figs. 4(a) and 4(c)], as expected from our intuitions [34, 36]. Since  $\mu_0H_{c2}^\varphi$  achieves its maximum for the field applied parallel to the  $[1\bar{1}0]$ -axis, and minimum for the directions  $90^\circ$  from the  $[1\bar{1}0]$ -axis, the superconducting gap leads to a maximum along the  $[1\bar{1}0]$ -axis and a minimum along the  $[11\bar{2}]$ -axis, whose topological contour is similar to that of  $sp$ -hybridization in molecule [37] [see the inset figure of Fig. 4(d)], signaling that the pairing symmetry of  $\text{YAlO}_3/\text{KTaO}_3$  most likely belongs to the  $s+p$ -wave.

Having experimentally established the asymmetric twofold anisotropy of the superconducting state of

$\text{YAlO}_3/\text{KTaO}_3$ , we now proceed to elaborate about its origin using the underlying symmetries of the crystal structure without requiring the details of the pairing mechanisms based on the group theoretical formulation of the Ginzburg-Landau theory [38]. This allows us to obtain fundamental information about the superconducting ground state in  $\text{YAlO}_3/\text{KTaO}_3$  superconductor. From the viewpoint of group symmetry, if a superconductor possesses an inversion symmetry, the Pauli principle requires a totally antisymmetric Cooper pair wavefunction, which imposes the condition that the superconducting states should be either spin-singlet or spin-triplet, whereas mixed-parity states are forbidden [38]. In the  $\text{YAlO}_3/\text{KTaO}_3$  the lack of inversion symmetry, however, tends to mix spin-singlet and spin-triplet driven by strong spin-orbit coupling [39]. Indeed, the conducting electrons with strong spin-orbit coupling originating from the heavy  $\text{Ta}$  5d orbitals has been revealed at  $\text{KTaO}_3$  interfaces [35, 40]. Due to the absence of a mirror plane parallel to the interface of  $\text{YAlO}_3/\text{KTaO}_3$ , the point group of  $\text{YAlO}_3/\text{KTaO}_3$  is  $C_{3v}$ , which does not contain the symmetry element of an inversion. This situation is analogue to non-centrosymmetric superconductors [39]. Upon inspecting the character table of  $C_{3v}$  point group listed in Table S1 [18], we notice that the mixed-parity superconducting state only belongs to the  $A_1+E$ -representation with the possible basis function of  $s+p$ . Interestingly, the two-dimensional irreducible representation of  $E$  can spontaneously break the threefold rotational symmetry of the crystal [see Fig. 1(c)], leading to a subsidiary uniaxial anisotropy [41], such as a uniaxial  $p_x$ -wave or  $p_y$ -wave pairing. Since the upper critical field is proportional to the superconducting gap amplitude [42],  $\mu_0H_{c2}^\varphi \propto |\Delta_{gap}(\varphi)|$ , only the  $s+p_x$ -wave pairing can give rise to an overall asymmetric twofold anisotropic gap shown in Fig. 4(c). In Fig. 4(d), we theoretically evaluate the mixed-parity superconducting gap  $|\Delta_{gap}|$  as a function of the ratio of  $s$ -wave  $\Delta_s$  and  $p$ -wave  $\Delta_p$  components,  $\gamma = \Delta_s/\Delta_p$ . In the two limiting cases of  $s$ -wave and  $p$ -wave pairing, the  $|\Delta_{gap}|$  exhibits isotropy and perfect twofold modulations, respectively. For increasing  $\gamma$ , the asymmetric anisotropy becomes more and more significant. These theoretical results are in qualitative agreement with the experimental observations shown in Fig. 4(c) (also see Fig. S5 [18]).

Therefore, we have evidence that the  $\text{KTaO}_3$  interface with inversion symmetry breaking represents an anisotropic mixed-parity superconductor with an admixture of  $s$ -wave and  $p$ -wave pairings driven by strong spin-orbit coupling. This is a relevant and appealing example obtained from heterostructure engineering of non-centrosymmetric bulk superconductors, and itself opens a new avenue to investigate unconventional superconductivity. In particular, it represents a novel platform to assess and clarify the emergence of unconventional superconductivity in systems showing a delicate interplay

of strong electron correlation and spin-orbit coupling, inherently linked to inversion symmetry breaking in the heterostructures.

*Acknowledgments.*—This work is supported by the National Natural Science Foundation of China (Grant Nos. 61871134 and 11927807) and Shanghai Science and Technology Committee (Grant Nos. 19ZR1402600 and 20DZ1100604). Y.S. is also sponsored by Shanghai Pujiang program (No. 20PJ1410900).

\* G. Zhang, L. Wang, and J. Wang contribute equally to this work.

† E-mail: songyr@shanghaitech.edu.cn

‡ E-mail: lijun3@shanghaitech.edu.cn

§ E-mail: w.li@fudan.edu.cn

---

[1] Y. Saito, T. Nojima, and Y. Iwasa, *Nature Reviews Materials* **2**, 16094 (2017).

[2] J. Mannhart and D. G. Schlom, *Science* **327**, 1607 (2010).

[3] P. Zubko, S. Gariglio, M. Gabay, P. Ghosez, and J.-M. Triscone, *Annu. Rev. Condens. Matter Phys.* **2**, 141 (2011).

[4] H. Y. Hwang, Y. Iwasa, M. Kawasaki, B. Keimer, N. Nagaosa, and Y. Tokur, *Nature Materials* **11**, 103 (2012).

[5] N. Reyren, Thiel, A. D. Caviglia, L. F. Kourkoutis, G. Hammerl, C. Richter, C. W. Schneider, T. Kopp, A.-S. Rüetschi, D. Jaccard, M. Gabay, D. A. Muller, J.-M. Triscone, J. Mannhart, *Science* **317**, 1196 (2007).

[6] A. Gozar, G. Logvenov, L. Fitting Kourkoutis, A. T. Bollinger, L. A. Giannuzzi, D. A. Muller, and I. Bozovic, *Nature* **455**, 782 (2008).

[7] Q.-Y. Wang, Z. Li, W.-H. Zhang, Z.-C. Zhang, J.-S. Zhang, W. Li, H. Ding, Y.-B. Ou, P. Deng, K. Chang, J. Wen, C.-L. Song, K. He, J.-F. Jia, S.-H. Ji, Y.-Y. Wang, L.-L. Wang, X. Chen, X.-C. Ma, and Q.-K. Xue, *Chin. Phys. Lett.* **29**, 037402 (2012).

[8] J.-F. Ge, Z.-L. Liu, C. Liu, C.-L. Gao, D. Qian, Q.-K. Xue, Y. Liu, and J.-F. Jia, *Nature Materials* **14**, 285 (2015).

[9] F.-C. Hsu, J.-Y. Luo, K.-W. Yeh, T.-K. Chen, T.-W. Huang, P. M. Wu, Y.-C. Lee, Y.-L. Huang, Y.-Y. Chu, D.-C. Yan, and M.-K. Wu, *Proc. Natl. Acad. Sci. U. S.A.* **105**, 14262 (2008).

[10] J. J. Lee, F. T. Schmitt, R. G. Moore, S. Johnston, Y.-T. Cui, W. Li, M. Yi, Z. K. Liu, M. Hashimoto, Y. Zhang, D. H. Lu, T. P. Devereaux, D.-H. Lee, and Z.-X. Shen, *Nature* **515**, 245 (2014).

[11] C. Liu, X. Yan, D. Jin, Y. Ma, H.-W. Hsiao, Y. Lin, T. M. Bretz-Sullivan, X. Zhou, J. Pearson, B. Fisher, J. S. Jiang, W. Han, J.-M. Zuo, J. Wen, D. D. Fong, J. Sun, H. Zhou, and A. Bhattacharya, *Science* **371**, 716 (2021).

[12] Y. Ma, J. Niu, W. Xing, Y. Yao, R. Cai, J. Sun, X. C. Xie, X. Lin, and W. Han, *Chin. Phys. Lett.* **37**, 117401 (2020).

[13] Z. Chen, Z. Liu, Y. Sun, X. Chen, Y. Liu, H. Zhang, H. Li, M. Zhang, S. Hong, T. Ren, C. Zhang, H. Tian, Y. Zhou, J. Sun, and Y. Xie, *Phys. Rev. Lett.* **126**, 026802 (2021).

[14] K. Ueno, S. Nakamura, H. Shimotani, H. T. Yuan, N. Kimura, T. Nojima, H. Aoki, Y. Iwasa, and M. Kawasaki, *Nature Nanotechnology* **6**, 408 (2011).

[15] P. Villar Arribi, A. Paramekanti, and M. R. Norman, *Phys. Rev. B* **103**, 035115 (2021).

[16] A. Biswas, C.-H. Yang, R. Ramesh, and Y. H. Jeong, *Progress in Surface Science* **92**, 117 (2017).

[17] Z. Chen, A. G. Swartz, H. Yoon, H. Inoue, T. A. Merz, D. Lu, Y. Xie, H. Yuan, Y. Hikita, S. Raghu, and H. Y. Hwang, *Nature Communications* **9**, 4008 (2018).

[18] See Supplemental Material for Materials and Methods, Figs. S1-S5, and Table S1.

[19] M. Tinkham, *Introduction to Superconductivity*, 2nd edn (McGraw-Hill, New York, 1996).

[20] B. S. Chandrasekhar, *Appl. Phys. Lett.* **1**, 7 (1962).

[21] A. M. Clogston, *Phys. Rev. Lett.* **9**, 266 (1962).

[22] M. Kim, Y. Kozuka, C. Bell, Y. Hikita, and H. Y. Hwang, *Phys. Rev. B* **86**, 085121 (2012).

[23] N. Reyren, S. Gariglio, A. D. Caviglia, D. Jaccard, T. Schneider, and J.-M. Triscone, *Appl. Phys. Lett.* **94**, 112506 (2009).

[24] Y.-L. Han, S.-C. Shen, J. You, H.-O. Li, Z.-Z. Luo, C.-J. Li, G.-L. Qu, C.-M. Xiong, R.-F. Dou, L. He, D. Naugle, G.-P. Guo, and J.-C. Nie, *Appl. Phys. Lett.* **105**, 192603 (2014).

[25] A. M. R. V. L. Monteiro, D. J. Groenendijk, I. Groen, J. de Bruijckere, R. Gaudenzi, H. S. J. van der Zant, and A. D. Caviglia, *Phys. Rev. B* **96**, 020504(R) (2017).

[26] J. Biscaras, N. Bergeal, A. Kushwaha, T. Wolf, A. Rastogi, R.C. Budhani, and J. Lesueur, *Nature Communications* **1**, 89 (2010).

[27] M. Tinkham, *Phys. Rev.* **129**, 2413 (1963).

[28] J. M. Lu, O. Zheliuk, I. Leermakers, N. F. Q. Yuan, U. Zeitler, K. T. Law, and J. T. Ye, *Science* **350**, 1353 (2015).

[29] L. Wang, H. Xue, G. Zhang, Z. Shen, G. Mu, S. Wu, Z. An, Y. Chen, and W. Li, *arXiv:2106.06948* (2021).

[30] D. Jiang, T. Yuan, Y. Wu, X. Wei, G. Mu, Z. An, and W. Li, *ACS Appl. Mater. Interfaces* **12**, 49252 (2020).

[31] J. M. Kosterlitz and D. J. Thouless, *J. Phys. Chem.* **5**, L124 (1972).

[32] M. R. Beasley, J. E. Mooij, and T. P. Orlando, *Phys. Rev. Lett.* **42**, 1165 (1979).

[33] B. I. Halperin and D. R. Nelson, *J. Low Temp. Phys.* **36**, 599 (1979).

[34] H. Xue, L. Wang, Z. Wang, G. Zhang, W. Peng, S. Wu, C. Gao, Z. An, Y. Chen, and W. Li, *arXiv:2110.13397* (2021).

[35] F. Y. Bruno, S. M. Walker, S. Riccò, A. de la Torre, Z. Wang, A. Tamai, T. K. Kim, M. Hoesch, M. S. Bahramy, and F. Baumberger, *Adv. Electron. Mater.* **5**, 1800860 (2019).

[36] A. Hamill, B. Heischmidt, E. Sohn, D. Shaffer, K.-T. Tsai, X. Zhang, X. Xi, A. Suslov, H. Berger, L. Forró, F. J. Burnell, J. Shan, K. F. Mak, R. M. Fernandes, K. Wang, and V. S. Pribiag, *Nature Physics* **17**, 949 (2021).

[37] M. S. Dresselhaus, G. Dresselhaus, and A. Jorio, *Group Theory: Application to the physics of condensed matter*, (Springer, Berlin Heidelberg, 2008).

[38] M. Sigrist and K. Ueda, *Rev. Mod. Phys.* **63**, 239 (1991).

[39] E. Bauer and M. Sigrist, *M. Non-centrosymmetric superconductors: Introduction and overview*, (Springer, Berlin Heidelberg, 2012)

[40] K. Rubi, S. Zeng, F. Bangma, M. Goiran, A. Ariando, W. Escoffier, and U. Zeitler, *Phys. Rev. Research* **3**, 033234

(2021).

[41] S. Yonezawa, *Condens. Matter* **4**, 2 (2019).

[42] J. D. Strand, D. J. Bahr, D. J. Van Harlingen, J. P. Davis, W. J. Gannon, and W. P. Halperin, *Science* **328**, 1368 (2010).